

Response Surface Optimization of Gamma Irradiation Synthesis of Alginate-Stabilized Silver Nanoparticles Without Addition of a Hydroxyl Radical Scavenger

D. P. Perkasa^{1,2*}, W. Arozal^{1,3}, Kusmardi^{1,4}, M. Syaifudin⁵

¹Doctoral Program in Biomedical Science, Faculty of Medicine, Universitas Indonesia, Jl. Salemba Raya No. 6, Jakarta 10430, Indonesia

²Research Center for Radiation Process Technology, Research Organization for Nuclear Energy - National Research and Innovation Agency, Jl. Lebak Bulus Raya No. 49, Jakarta 12440, Indonesia

³Dept. of Pharmacology and Therapeutics, Faculty of Medicine, Universitas Indonesia, Jl. Salemba Raya No. 6, Jakarta 10430, Indonesia

⁴Dept. of Pathological Anatomy, Faculty of Medicine, Universitas Indonesia, Jl. Salemba Raya No. 6, Jakarta 10430, Indonesia

⁵Research Center for Radioisotope, Radiopharmaceutical, and Biodosimetry Technology, Research Organization for Nuclear Energy - National Research and Innovation Agency, Puspitpek Area Serpong, Tangerang Selatan 15310, Indonesia

ARTICLE INFO

Article history:

Received 30 July 2021

Received in revised form 22 April 2022

Accepted 1 July 2022

Keywords:

Silver nanoparticles

Alginate

Gamma irradiation

Response surface methodology

Optimization

ABSTRACT

The use of isopropanol as a hydroxyl radical scavenger on the radiosynthesis of alginate-stabilized silver nanoparticles (AgNPs) can limit its application in nanomedicine. Meanwhile, optimum condition for gamma irradiation synthesis of alginate-stabilized AgNPs without addition of a hydroxyl radical scavenger has not been reported yet. In this study, the optimization of this process was carried out using response surface methodology (RSM) combined with Central Composite Design (CCD). The three processing conditions, i.e. radiation dose, precursor silver ion concentration, and alginate concentration were selected as decision variables to maximize two responses in terms of the conversion yield and AgNP concentration responses. The results indicated that the regression model of conversion yield and AgNP concentration fit linearly with the two-factor interaction and the linear model, respectively. The significant effect of the alginate factor on the conversion yield indicates the dual stabilizing–scavenging role of the alginate. The optimum conditions derived from CCD-RSM were obtained at a 20 kGy radiation dose, 7.78 mM precursor silver ion concentration, and 1.2 % (w/v) alginate concentration with the desirability of 0.731. The actual experimental results were 65.43% conversion yield and 480.91 ppm AgNP concentration, which were within the prediction interval at confidence of 95 %. The AgNPs under the optimum condition had a spherical shape, 97.4 % volume of size distribution at 6.50-28.21 nm, and zeta potential of -28.3 mV.

© 2022 Atom Indonesia. All rights reserved

INTRODUCTION

Nanotechnology is an emerging technology in the medical area with promising applications in the treatment and prevention of chronic diseases [1,2]. In particular, silver nanoparticles (AgNPs) have been extensively investigated because of their anti-inflammatory activity [3-6]. *In vivo* studies

reported that the presence of AgNPs led to lower concentration of pro-inflammatory cytokines [3,4,7], faster intestinal tissue healing after injury [4], a decrease in the activity of matrix metalloproteinase-9 [7], and a reduction in tissue myeloperoxidase activity accompanied by decreased microscopic and microscopic damage score [5,6]. AgNPs also suppress expression of COX-2 and HIF-1 α and decrease the production of VEGF [1].

For application in nanomedicine, it is important to develop colloidal AgNPs with high

*Corresponding author.

E-mail address: dpribadi@batan.go.id

DOI: <https://doi.org/10.17146/aij.2022.1169>

purity, particularly from the residue of the precursor of a reaction system. Colloidal AgNPs are typically synthesized through a bottom-up approach in which reaction system typically contains three main components, i.e., metal precursor, reducing agent, and stabilizing agent. Various routes have been established for the synthesis of AgNPs [8]. Among them, the gamma radiosynthesis offers unique benefits. Firstly, Ag^+ ions are reduced to uncharged state of Ag^0 by reducing radicals produced by radiolysis of water. Thus, there is no issue about potential toxicity of the residual reducing agent [9], which ensures its biocompatibility for application in the biomedical field. Also, gamma radiosynthesis operates under simple physicochemical conditions that allow homogeneous reduction and nucleation of AgNPs [10,11]. However, radiosynthesis requires the addition of isopropanol as a hydroxyl radical scavenger to improve the reduction capacity of irradiation processing [12].

The use of isopropanol in radiosynthesized alginate-stabilized AgNPs has been reported [13]. Alginate is a collective term for linear anionic polysaccharides composed of 1,4-linked β -D-mannuronic acid and α -L-guluronic acid residues [14,15]. Based on Liu *et al.* [13], alginate was a biocompatible stabilizing agent due which maintained the dispersion stability for over 6 month at room temperature. Radiosynthesized alginate-stabilized AgNPs also showed higher antimicrobial activity compared to other stabilizer, such as polyvinyl pyrrolidone, polyvinyl alcohol dan sericin [16]. However, optimum radiosynthesis conditions have not been reported yet.

This study was aimed at optimizing three operation factors for gamma irradiation synthesis of alginate-stabilized AgNPs without addition of a hydroxyl radical scavenger, particularly isopropanol. The use of isopropanol is avoided in this study because it exhibits toxicity to the central nervous system [17]. Alcohol consumption is also prohibited by the law of Islam, which is the religion of the majority of Indonesian citizen. Along with alginate concentration, irradiation dose and precursor silver ion concentration would be optimized by employing Central Composite Design-Response Surface Methodology (CCD-RSM) methods to obtain the optimum condition for the conversion yield and AgNPs concentration responses.

METHODOLOGY

Materials

The silver nitrate salt (>99.8 % purity, Merck, Germany) was used as a silver ion precursor to

produce AgNPs, whereas the sodium alginate (molecular biology grade, HiMedia, India) was used as a liquid medium of colloidal AgNPs. The calcium nitrate tetrahydrate (analytical grade, Merck, Germany) was used as a desolvating agent of AgNPs prior to sedimentation by centrifugation. The nitric and hydrochloric acids (Merck, Germany) were of analytical grade for use in wet digestion for elemental analysis.

Instrumentation

Gamma irradiation was carried out at Research Center for Radiation Process Technology, Research Organization for Nuclear Energy - National Research and Innovation Agency, Indonesia, using a Co-60 gamma ray irradiator (series Gammacell 220, MDS Nordion, Canada). After irradiation, the occurrence of AgNPs within reaction systems was detected based on their localized surface plasmon resonance (ISPR) using a UV-Vis spectrophotometer (series Cary100, Agilent, US). The centrifuge (series Heraeus Biofuge Primo R, Thermo Fisher Scientific, US) was used in separation of AgNPs from residual silver ion. The silver content was quantified using a flame atomic absorption spectrometer (FAAS; series 240FS AA, Agilent, US) at Research Center for Nuclear Fuel Cycle and Radioactive Waste Technology, Research Organization for Nuclear Energy - National Research and Innovation Agency, Indonesia. The instruments for characterization of colloidal AgNPs were a transmission electron microscope (TEM; series JEM-1400, JEOL, Japan), dynamic light scattering (DLS; series Zetasizer Nano, Malvern Panalytical Ltd., UK), a Fourier transform infrared spectrophotometer (FTIR; series IRPrestige21, Shimadzu, Japan), and an X-ray diffractometer (XRD; series Empyrean, Malvern Panalytical Ltd., UK).

Stock solution and sample preparation

Twenty-five milliliters of a 0.2 M AgNO_3 stock solution was prepared by dissolving 0.85 g of an AgNO_3 crystal (169.8731 g/mol) in ultrapure water using a 25 mL volumetric flask until the water volume reached 25 mL. The AgNO_3 stock was prepared at room temperature under a dark condition to prevent photochemical reaction. The alginate solutions were prepared by dissolving sodium alginate powder in ultrapure water at room temperature for 4 hours under continuous stirring.

Experimental design of radiosynthesis

Each reaction system was a certain volume of the 0.2 M AgNO₃ solution blended with 40 ml of the alginate solution that was prepared in a screw-capped bottle under the dark condition. The reaction systems were homogenized by vortexing for 20 s. Neither nitrogen bubbling treatment nor isopropanol addition was applied to the reaction systems. Soon after preparation, the reaction systems were irradiated using a Co-60 gamma ray irradiator at various doses and a fixed dose rate of 5 kGy/h. The radiation processing was conducted at ambient temperature under atmospheric gases and pressure. Successful conversion of silver ion into AgNPs was detected colorimetrically using a UV-Vis spectrophotometer based on the occurrence of localized surface plasmon resonance (ISPR) absorption that peaked at approximately 400 nm. Measurements were conducted using a 1 cm path length quartz cuvette at a wavelength of 200-800 nm at 1 nm resolution. Then, the colloidal AgNPs from all experimental runs were stored at 4°C under a dark condition until they were used for further experiments.

The CCD-RSM was applied to determine the optimal condition of irradiation dose (X1), silver ion precursor concentration (X2), and alginate concentration (X3) for conversion yield (response 1) and AgNP concentration (response 2). Each of experimental factors has five levels, as presented in Table 1. The experiment consisted of 20 trial runs involving 8 center points, 8 factorial points, and 4 axial points.

Table 1. Experimental factors with five levels for CCD-RSM.

Variable (unit)	Levels				
	Minimum (-√3)	Low (-1)	Center (0)	High (1)	Maximum (√3)
X1: Radiation dose (kGy)	3.91	8.00	14.00	20.00	24.09
X2: [Ag ⁺ precursor] (mM)	1.27	4.00	8.00	1.20	14.73
X3: [Alginate] (%)	0.13	0.40	0.80	1.20	1.47

The total silver and silver ion concentrations were measured based on procedure reported by Dong *et al.* [18] with modification using FAAS. Briefly, the sample for total silver measurement was prepared by acidifying 1 mL of each colloidal AgNP with 9 mL of 67 % (w/w) HNO₃ overnight at room temperature. Then, the digested suspension was diluted with ultrapure water to a final HNO₃ concentration of 0.2 % (w/v). The sample for silver ion measurement was prepared by pre-treating 5 mL of each colloidal AgNP with 5 ml of a 4 % (w/v) calcium nitrate solution followed by centrifugation

at 1,000 × g for 10 minutes. Then, the supernatant was carefully collected for silver ion analysis. The conversion yield and AgNP concentration were calculated using Eqs. (1) and (2), respectively:

$$Yield (\%) = \frac{[Total\ silver] - [Silver\ ion]}{[Total\ silver]} \times 100\% \quad (1)$$

$$[AgNPs] (ppm) = [Total\ silver] - [Silver\ ion] \quad (2)$$

The results of the experiment were analyzed using DesignExpert (trial version 6.0.4 for academic use, StatEase Inc., US) software. The functional relationship between response and the set of operation factors was determined using regression model. The significance of the model and the regression coefficient was evaluated using analysis of variance.

Multiple response optimization and model validation

Multiple response optimization was employed to determine the optimum operating conditions for several responses simultaneously using the desirability function. The desirability function converts each estimated response (\hat{Y}_i) into a scale-free value. It is called desirability and is denoted as d_i for \hat{Y}_i . The value of desirability of an individual function varies over the range 0 to 1; $d_i(\hat{Y}_i) = 1$ represents a completely desirable response, whereas $d_i(\hat{Y}_i) = 0$ is a completely undesirable response [19]. As presented in Table 5, both responses were to be maximized. Therefore, the individual desirability was defined as Eq. (3):

$$d_i(\hat{Y}_i) = \begin{cases} 0 & \text{if } \hat{Y}_i(x) < L_i \\ \left(\frac{\hat{Y}_i(x) - L_i}{T_i - L_i}\right)^{1/k} & \text{if } L_i \leq \hat{Y}_i(x) \leq T_i \\ 1 & \text{if } \hat{Y}_i(x) > T_i \end{cases} \quad (3)$$

where L_i , U_i , and T_i are the lower, upper, and target values, respectively, with T_i interpreted as a large enough value for the response. Then, the individual desirabilities were combined using a geometric mean, which gave the overall desirability (D) as indicated in Eq. (4):

$$D = (d_1(\hat{Y}_1)d_2(\hat{Y}_2) \dots d_k(\hat{Y}_k))^{1/k}, \quad (4)$$

with k denoting the number of responses. The value of desirability increases as the corresponding response value becomes more desirable [19,20]. The deviation of the predicted value from the actual

value was calculated as the mean percentage error (MPE) using Eq. (5):

$$MPE = \frac{100\%}{n} \sum_{t=1}^n \frac{a_t - f_t}{a_t}, \quad (5)$$

where a_t is the actual value, f_t is the predicted value, and n is the number of different times for which the variable is predicted. The MPE value is interpreted as a highly accurate forecasting if < 10 , a good forecasting if $10 - 20$, a reasonable forecasting if $20 - 50$, and an inaccurate forecasting if > 50 [21].

Characterization of AgNPs at the optimum condition

Colloidal AgNPs under the optimum condition was characterized for its conversion yield and AgNP concentration based on previously described procedures [18]. Further, colloidal AgNPs under the optimum condition was characterized for particle size and morphology using TEM. Then, the TEM micrographs were processed and analyzed using the ImageJ (ver. 1.51i, developed by Wayne Rasband, National Institute of Health, USA) software. The hydrodynamic size and zeta potential were characterized using the DLS instrument. The FTIR spectrum of the freeze-dried AgNP sample was measured at $4,000-400 \text{ cm}^{-1}$ at 2 cm^{-1} resolution. The crystal structures of AgNPs were characterized using XRD.

RESULTS AND DISCUSSION

Results indicated that the reaction system underwent color alteration after gamma ray irradiation. As seen in Fig. 1, it changed from transparent colorless to transparent yellowish brown. As reported elsewhere [22,23], the yellowish brown color indicates the formation of colloidal AgNPs. The distinctive color of AgNPs is the result of ISPR absorption in the visible spectrum, which is an intense and broad optical absorption band that started at 320 nm from a strong coherence oscillation of conduction electrons near the surface of AgNPs [22,23]. Accordingly, the UV-Vis spectra in Fig. 1 confirmed that the ISPR of AgNPs was within the visible wavelength from 300 to 550 nm; this means they reflect the yellow spectrum but absorb the red and blue spectra.

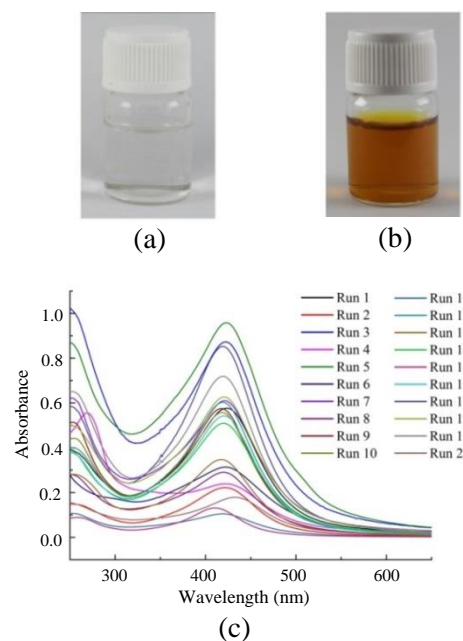
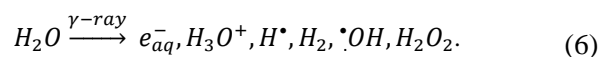


Fig. 1. (a) Appearance of the reaction system before; (b) after irradiation, and (c) the UV-Vis spectra (right) of colloidal AgNPs.

As seen in Fig. 1, the UV-Vis spectra of AgNPs exhibited a single intense ISPR absorption peak at approximately 420 nm. Bastús *et al.* [24] reported that the ISPR vibration mode of AgNPs was sensitively influenced by particle morphology. The single ISPR peak only occurs for spheroid AgNPs with an average size below 67 nm, which corresponds to the dipolar plasmon vibration mode. When the size of AgNPs increases above the size of 67 nm, a new peak starts to develop at shorter wavelengths ($\sim 400 \text{ nm}$) corresponding to quadrupole vibration of the plasmon resonance. The quadrupole vibration occurs because light cannot polarize homogeneously and the field is no longer uniform throughout the nanoparticles [24]. Based on these reports, the UV-Vis spectra in Fig. 1 indicate that the silver particle from each experimental run is at nano scale. Thus, an alginate within a range of 0.13 % - 1.47 % can play a role as a stabilizing agent for radiosynthesis of AgNPs.

The gamma irradiation of a polysaccharide solution containing a metal ion precursor leads to generation of zero-valent metal atoms through an indirect effect. The radiation energy is mostly absorbed by water molecules, whereas the absorption by the metal ion precursor and dissolved polymer can be neglected [25]. Then, radiolysis of water occurs and generates a large number of radicals; it is simplified as implied in Eq. (6):



These reactive species are created in very high concentration and begin to migrate randomly about

their initial positions. As diffusion proceeds, a variety of reactions are possible in the diffusion tract. Solvated electron (e_{aq}^-) and hydrogen radicals (H^\bullet) are strong reducing agents that can reduce silver ions into zero-valent silver atoms. By contrast, hydroxyl radical ($^\bullet OH$) and dissolved oxygen are strong oxidizing agents that can oxidize silver atom into silver ion [10,25]. Since reduction and oxidation reactions occur randomly during the irradiation processing, the statistical optimization of the experimental conditions is critical in development of synthesis methods [26,27].

Table 2 presents the factors and responses and their results from 20 runs of CCD-RSM. On the basis of the experimental result, the regression equation in Table 3 was developed to illustrate the empirical relationships between factors and each response. The regression coefficients for response surface models were statistically tested for their significance using analysis of variance (ANOVA), as presented in Table 3. Based on the regression model, the response surface plots of conversion yield and AgNP concentration are visualized in Fig. 2.

Table 2. The CCD-RSM with experimental response of conversion yield and AgNP concentration.

Run	Factors in coded level			Factors in actual value			Responses	
	X1	X2	X3	X1	X2	X3	Response 1: Yield (%)	Response 2: [AgNPs] (ppm)
1	24.09	8	0.8	$\sqrt{3}$	0	0	69.62	697.97
2	20	4	1.2	-1	-1	1	78.22	278.87
3	14	14.73	0.8	0	$\sqrt{3}$	0	49.07	828.29
4	14	8	0.8	0	0	0	24.52	229.80
5	8	12	0.4	-1	1	-1	73.63	953.96
6	14	8	0.13	0	0	$-\sqrt{3}$	24.58	232.72
7	3.91	8	0.8	$-\sqrt{3}$	0	0	46.96	440.96
8	8	4	1.2	-1	-1	1	51.99	228.39
9	14	8	0.8	0	0	0	55.83	504.97
10	14	8	0.8	0	0	0	53.36	425.99
11	8	4	0.4	-1	-1	-1	26.89	72.26
12	14	8	0.8	0	0	0	54.18	482.66
13	14	8	0.8	0	0	0	55.40	462.61
14	8	12	1.2	-1	1	1	57.44	670.26
15	14	1.27	0.8	0	$-\sqrt{3}$	0	74.74	104.48
16	14	8	0.8	0	0	0	56.44	474.95
17	20	12	1.2	1	1	1	66.22	765.89
18	20	12	0.4	1	1	-1	38.30	440.32
19	14	8	1.47	0	0	$\sqrt{3}$	64.30	520.72
20	20	4	0.4	1	-1	-1	55.16	230.26

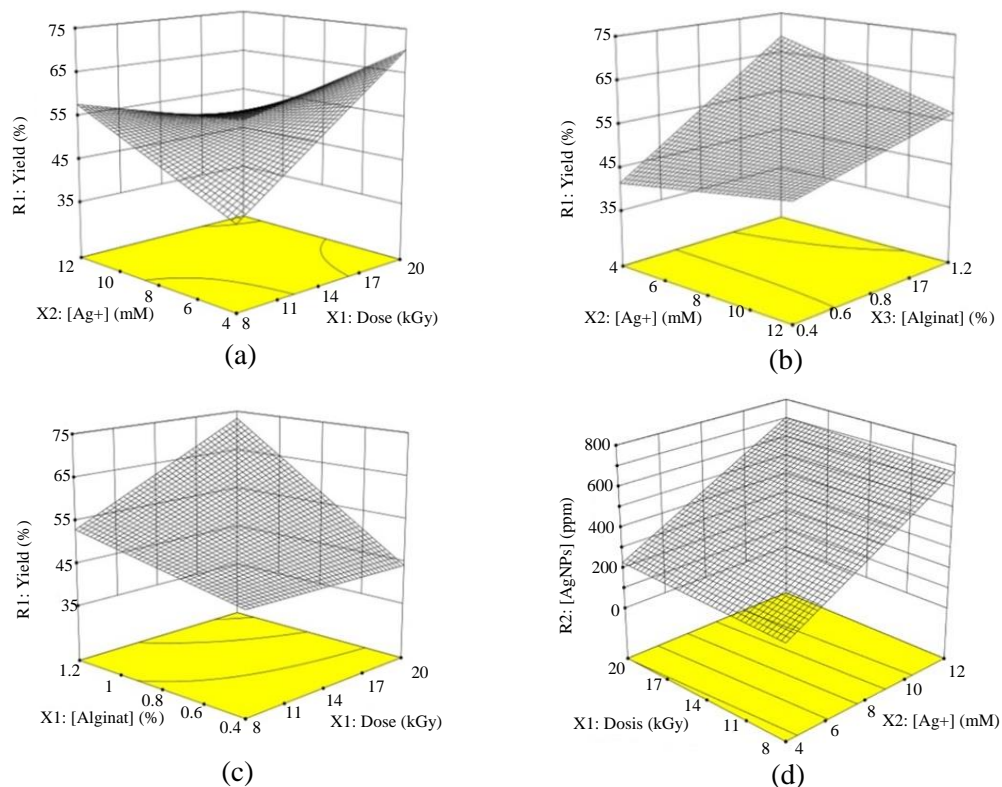


Fig. 2. Response surface plots of the conversion yield (left and top right) and AgNP concentration (bottom right) at constant (a, d) alginate concentration (0.8 %), radiation dose (14 kGy), (b) silver ion precursor (8 mM), and (c) radiation dose (14 kGy).

Table 3. The ANOVA for response surface models.

Response	Source	Sum of square	Degree of freedom	Mean square	F-value	p-value
Yield	Linear two-factor interaction model	2,732.38	6	455.40	2.98	0.0496*
	Residual	1,989.46	13	153.04		
	Lack of fit	1,207.06	8	150.88	0.96	0.5425
	Pure error	782.40	5	156.48		
	Total	4,721.85	19			
[AgNPs]	Linear Model	8.10×10^5	3	2.70×10^5	14.83	<0.0001*
	Residual	2.91×10^5	16	1.82×10^4		
	Lack of fit	2.39×10^5	11	2.18×10^4	2.11	0.2110
	Pure Error	5.16×10^4	5	1.03×10^4		
	Total	1.10×10^6	19			

* Significant at a confidence interval of 95 % because the p-value is less than 0.05

Table 4. The sequential model sum of square of the regression models for yield response.

Source	Sum of Squares	df	Mean Square	F Value	p-value Prob > F	
Mean vs Total	57983.79	1	57983.79		Suggested	
Linear vs Mean	1522.10	3	507.37	2.54	0.0933	
2FI vs Linear	1210.29	3	403.43	2.64	0.0937	Suggested
Quadratic vs 2FI	471.68	3	157.23	1.04	0.4181	
Cubic vs Quadratic	733.28	4	183.32	1.40	0.3382	Aliased
Residual	784.50	6	130.75			
Total	62705.64	20	3135.28			

Table 5. The lack of fit test of the regression models for yield response.

Source	Sum of Squares	df	Mean Square	F Value	p-value Prob > F	
Linear	2417.35	11	219.76	1.40	0.3729	
2FI	1207.06	8	150.88	0.96	0.5425	Suggested
Quadratic	735.38	5	147.08	0.94	0.5263	
Cubic	2.10	1	2.10	0.013	0.9122	Aliased
Pure Error	782.40	5	156.48			

Table 6. The R-squared of the regression models for yield response.

Source	Std. Dev.	R-Squared	Adjusted R-Squared	Predicted R-Squared	PRESS	
Linear	14.14	0.3224	0.1953	-0.1204	5290.47	
2FI	12.37	0.5787	0.3842	-0.2760	6024.89	Suggested
Quadratic	12.32	0.6786	0.3893	-0.5105	7132.12	
Cubic	11.43	0.8339	0.4739	0.6634	1589.50	Aliased

Table 7. The R-squared of the response surface 2FI model of yield response.

Std. Dev.	12.37	R-Squared	0.5787
Mean	53.84	Adj R-Squared	0.3842
C.V. %	22.98	Pred R-Squared	-0.2760
PRESS	6024.89	Adeq Precision	7.871
-2 Log Likelihood	148.76	BIC	169.73
		AICc	172.09

Table 8. The sequential model sum of square of the regression models for [AgNPs] response.

Source	Sum of Squares	df	Mean Square	F Value	p-value Prob > F	
Mean vs Total	4.092E+006	1	4.092E+006			
Linear vs Mean	8.105E+005	3	2.702E+005	14.83	<0.0001	Suggested
2FI vs Linear	83845.49	3	27948.50	1.75	0.2061	
Quadratic vs 2FI	41205.93	3	13735.31	0.83	0.5092	
Cubic vs Quadratic	1.137E+005	4	28423.03	3.24	0.0967	Aliased
Residual	52643.54	6	8773.92			
Total	5.194E+006	20	2.597E+005			

Table 9. The lack of fit test of the regression models for [AgNPs] response.

Source	Sum of Squares	df	Mean Square	F Value	p-value Prob > F	
Linear	2.398E+005	11	21801.17	2.11	0.2110	Suggested
2FI	1.560E+005	8	19495.93	1.89	0.2504	
Quadratic	1.148E+005	5	22952.30	2.23	0.2003	
Cubic	1069.37	1	1069.37	0.10	0.7605	Aliased
Pure Error	51574.16	5	10314.83			

Table 10. The R-squared of the response surface linear model of [AgNPs] response.

Std. Dev.	134.95	R-Squared	0.7355
Mean	452.31	Adj R-Squared	0.6860
C.V. %	29.84	Pred R-Squared	0.5460
PRESS	5.002E+005	Adeq Precision	13.214
-2 Log Likelihood	248.49	BIC	260.47
		AICc	259.16

As seen in Table 3, the regression model for each response was statistically fit. The regression equation for response 1 was linear with a two-factor interaction model (Tables 4-6). The model p-value implies that the model was significant where there was only a 4.69 % chance that an F-value could occur because of noise. Also, the good predictability of the model was confirmed by a non-significant lack of fit where there was a 54.25 % chance that the lack of fit could occur because of noise (Table 6). The adequate precision in Table 7 measured the signal to noise ratio, which was at 7.87, indicates an adequate signal. Meanwhile, the regression equation for response 2 followed linear model (Tables 8-10). Based on its p-value, the model was significant where there was only less than 0.01 % chance that an F-value could occur because of noise. The good predictability of the model was confirmed by a non-significant lack of fit where there was a 21.10 % chance that the lack of fit could occur because of noise (Table 10). The adequate precision in Table 10 measured the signal

to noise ratio, which was at 13.21 indicates an adequate signal. The normal probability plots of the studentized residuals of both response showed the normality of residuals (Figs. 3 and 4).

As seen in Table 11, response 2 was significantly influenced by factor X2 with an estimated positive effect of 237.09. Meanwhile, the X1 and X3 factors have not been significantly affected. While, the ANOVA for regression coefficients of response 1 indicated that only the linear X3 and interaction X1*X2 factors had a significant effect, as seen in Table 11. The alginate concentration has the most significant effect (p -value = 0.0159) on the conversion yield with estimated effects of 7.05, followed by the interaction effect between the dose rate and precursor silver ion concentration (p -value = 0.0374) with estimated effects of -10.14. Note that the positive values of coefficient estimates indicate positive influence of the factor of the reaction, whereas the negative values estimates indicate negative influence. As seen in Figs. 2(c), 2(d); increasing the alginate concentration increased the conversion yield at any X1 and X2 value. Previously, an alginate was only reported as a stabilizing agent during radiosynthesis of AgNPs [16]. Indeed, antioxidant activity of a gamma-irradiated alginate has been reported against the 1,1-diphenyl-2-picrylhydrazyl and superoxide free radicals [28]. Therefore, these results proved that an alginate can act as a stabilizing agent and a hydroxyl radical scavenger agent during radiosynthesis of AgNPs.

Figure 2(a) illustrates 3D response surface plot of the conversion yield as a function of radiation dose and precursor silver ion concentration at a fixed alginate concentration of 0.8 %. The plot appeared in saddle-shape with a stationary area in the middle. Increasing the combined effect between radiation dose and the precursor silver ion concentration generally decreased the conversion yield. It seems that the efficiency of the reduction process by water radiolysis product is low when the silver ion precursor concentration is high. As seen in Fig. 2(a), the highest conversion yield was achieved when the radiation dose was at maximum, while the precursor silver ion concentration is at minimum. However, the optimization process is critical to obtaining the optimum combined effect of the radiation dose and precursor silver ion concentration on conversion yield.

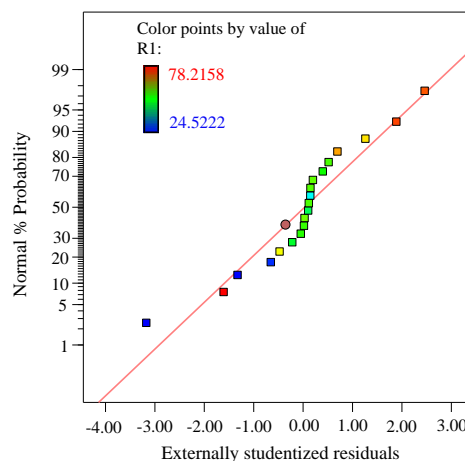


Fig. 3. The normal probability plot of the studentized residual for response surface 2FI model of yield response.

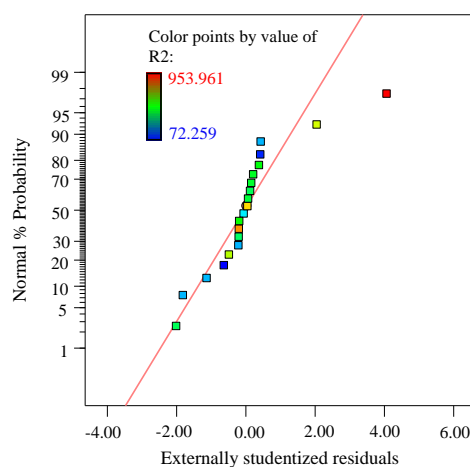


Fig. 4. The normal probability plot of the studentized residual for response surface 2FI model of [AgNPs] response.

Table 11. Regression coefficients for response surface models.

Response	Factors	Coefficient		p-values
		Coded level	Actual value	
Yield	Intercept	53.84	-14.06	-
	X1	4.83	2.43	0.1725
	X2	-1.45	7.83	0.6720
	X3	9.27	15.28	0.0159*
	X1*X2	-10.14	-0.42	0.0374*
	X1*X3	5.26	2.19	0.2502
	X2*X3	4.56	-2.85	0.3161
[AgNPs]	Intercept	452.31	-166.97	-
	X1	16.31	2.72	0.6612
	X2	237.09	59.27	<0.0001*
	X3	53.52	133.81	0.1621

* Significant at a confidence interval of 95 % because the p -value is less than 0.05

In Table 11, it is seen that the ANOVA for regression coefficients of response 2 indicated that only the linear X2 has a significant effect (p -value < 0.001) on the AgNP concentration with estimated effects of 237.09. As seen in Fig. 2(d), the 3D response surface plot of the AgNP concentration as a function of the radiation dose and precursor silver

ion concentration at a fixed alginate concentration of 0.8 % appeared in a flat plane. Increasing the precursor silver ion concentration enlarged the AgNP concentration after gamma irradiation.

The main objective of this study was to determine the optimal operation parameters for radiosynthesis of alginate-stabilized AgNPs. In this study, a simultaneous multiple response model was developed using CCD-RSM with a desirable function. The conversion yield and AgNP concentration were set at maximum values; values of process variables were set in the range under study, whereas the optimized parameters were selected based on the highest desirability. The optimization constrain generated a solution with a desirability at 0.731, as illustrated in Table 12.

To validate the statistical experiment strategies, the triplicate AgNP radiosynthesis was performed under the predicted process condition. The optimum condition of conversion yield and AgNP concentration were achieved at a radiation dose, precursor silver ion concentration, and alginate concentration of 20 kGy, 7.78 mM, and 1.2 %, respectively. As presented in Table 13, the simultaneous multiple response model has been validated to demonstrate significantly good agreement between the experimental value and the predicted value at a confidence interval of 95 %. The conversion yield and AgNP concentration were 65.43 % (MPE = -13.32 %) and 480.91 ppm (-5.54 %), respectively. The MPE values indicated the good forecasting and the highly accurate forecasting for conversion yield and AgNPs concentration responses, respectively.

Table 12. Multiple response optimization for conversion yield and AgNP concentration.

Criteria	Optimization Parameter			Prediction
	Goal	Lower Limit	Upper Limit	
Radiation dose (kGy)	In range	8.00	20.00	20.00
Ag ⁺ precursor (mM)	In range	4.00	12.00	7.78
Alginate (%)	In range	0.40	1.20	1.20
Yield (%)	Maximize	24.52	78.22	74.10
[AgNPs] (ppm)	Maximize	72.26	953.96	509.14

Note: Desirability value (D) = 0.731

Table 13. Post-analysis confirmation of the multiple response model at the optimum condition.

Response	Predicted Mean	Standard Error Prediction	Experiment		MPE (%)	Prediction Interval at a confidence of 95 %	
			Data	Mean		Low Limit	High Limit
			Yield	74.10		10.02	64.69 67.66 63.93
[AgNPs]	509.14	300.87	475.50 497.33 469.91	480.91	-5.54	300.87	717.42

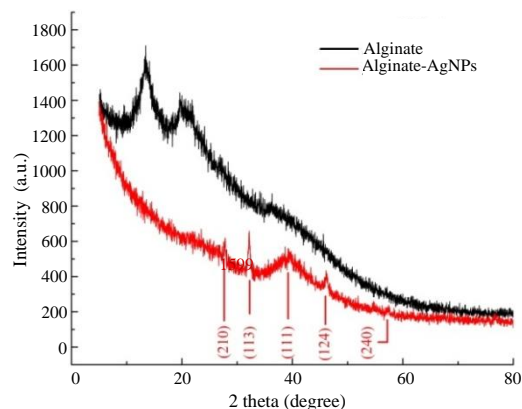


Fig. 5. X-ray diffractogram of the alginate and alginate-stabilized AgNPs.

The desirability value and the good agreement between the model and experimental values confirmed the applicability of the multiple response model. However, considering the MPE values, improvement on the precision of the model may be achieved in further research through the model reduction from insignificant factors.

Properties of the AgNPs synthesized under the optimum condition were characterized with Cu_{Kα} irradiation ($\lambda = 1.5412 \text{ \AA}$). The X-ray diffractograms in Fig. 5 confirm the materials obtained are sodium alginate and alginate-stabilized AgNPs. The diffractogram of sodium alginate showed a baseline shift at lower 2θ with several broadened peaks at 2θ below 20° . This result indicates that sodium alginate used in this study has a semi-crystalline nature. By contrast, the alginate-stabilized AgNPs samples showed Bragg's 2θ angles at 27.9° , 32.3° , 38.6° , 46.1° , and 57.4° which are indexed as (210), (113), (111), (124), and (240) crystal planes of the face centered cubic structure, respectively. A similar XRD pattern was reported on the green synthesized AgNPs prepared by *Caranthus roseus* and *Azadirachta indica* extracts in which the lattice planes were confirmed and cross-checked with the standard peak JCPDS database numbers 84-0173 and 04-0783 [29]. However, the Bragg's 2θ angles in this study were broadened with low intensity, which indicated that AgNPs are at low crystallinity.

The FTIR measurements were made to identify the functional group of the materials. As illustrated in Fig. 6, the FTIR spectrum of alginate indicates characteristic of O-H stretching vibration between $3,600$ and $3,200 \text{ cm}^{-1}$, asymmetric COO^- stretching vibration at $1,604 \text{ cm}^{-1}$, symmetric COO^- stretching vibration at $1,415 \text{ cm}^{-1}$, and C-O-C stretching vibration at $1,032 \text{ cm}^{-1}$ [30]. Compared to the FTIR spectrum

of the alginate, the alginate-stabilized AgNPs indicate only minor changes in the pattern and position of the absorption band. They exhibit the position shift in the absorption peaks of the asymmetric COO⁻ stretching vibration (from 1,604 to 1,599 cm⁻¹) and the symmetric COO⁻ stretching vibration (from 1,415 to 1,417 cm⁻¹). As reported elsewhere [31], these shifts confirm that AgNPs have been capped by a lone pair electron around the oxygen atoms in carboxyl group of the alginate through van der Waals interaction force. However, there is a differential peak at 1,384 sourced from the nitro group from the silver nitrate precursor [32].

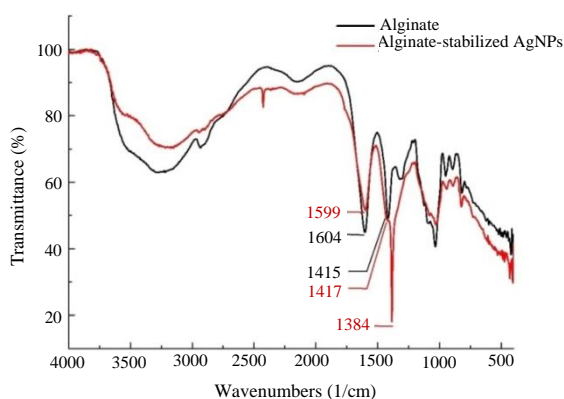
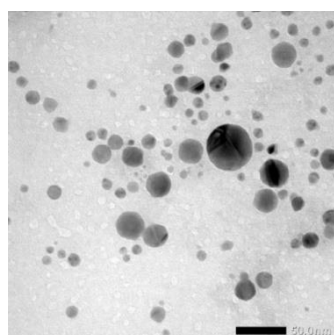


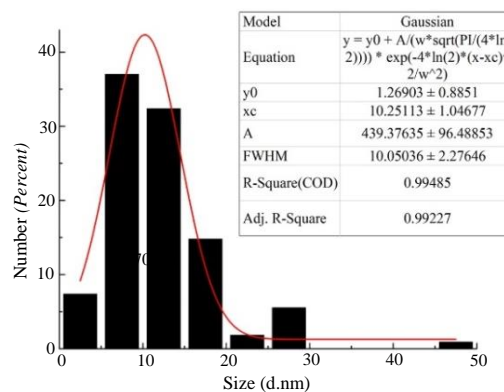
Fig. 6. FTIR spectra of the alginate and alginate-stabilized AgNPs.

The TEM imaging showed that alginate-stabilized AgNPs had a spherical shape with smooth edges, as presented in Fig. 7. Processing on the TEM micrograph revealed that the AgNPs had a diameter size of 10.25 ± 5.03 nm (Adj. R2 = 0.99). However, there was some particles with diameter between 20 and 50 nm. As illustrated in Fig. 8, the DLS measurement showed that the 97.4 % volume of particles was at a hydrodynamic size of 6.50-28.21 nm. The average hydrodynamic size was at 18.62 nm, higher than that in the TEM results, because of the occurrence of a dielectric layer at the interface of particles and solution. By contrast, the 2.4 % volume of particles was at a size range of 3,091-7,456 nm, which seems to be contaminated by dust particles.

The zeta potential measurement indicates the stability of alginate-stabilized AgNPs in aqueous suspension. Figure 8 presents the results of zeta potential analysis of the as-synthesized alginate-stabilized AgNPs at the optimum operation condition. The AgNPs exhibited a negative zeta potential at a value of -28.3 mV, which is in the range required for a stable suspension. This finding clearly indicates that the carboxyl pendant group of the alginate stabilizes AgNPs with high negative surface charges. The negative charge provides AgNPs with electrostatic repulsion to prevent aggregation.

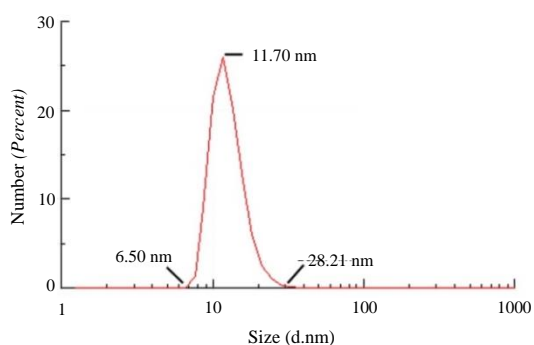


(a)

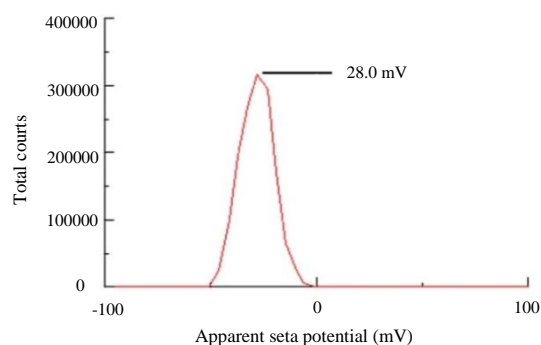


(b)

Fig. 7. (a) TEM micrograph, and (b) particle size distribution of the alginate-stabilized AgNPs.



(a)



(b)

Fig. 8. (a) Hydrodynamic size, and (b) zeta potential distributions of the alginate-stabilized AgNPs.

CONCLUSION

This study successfully synthesized the alginate-stabilized AgNPs using gamma irradiation without addition of a hydroxyl scavenger. Response surface modeling was successfully combined with CCD to determine the individual effect and combined effect of three processing conditions, i.e., radiation dose, precursor silver ion concentration and alginate concentration, on the conversion yield and AgNP concentration. The most significant factor that affects the conversion yield was found to be alginate concentration; this indicated the dual stabilizing-scavenging role of the alginate during radiosynthesis. The optimum conditions of conversion yield and AgNP concentration were achieved at a radiation dose, precursor silver ion concentration, and alginate concentration of 20 kGy, 7.78 mM, and 1.2 %, respectively, with the desirability of 0.731. Under these conditions, the maximum conversion yield of 65.43 % and AgNP concentration of 480.91 ppm were obtained. The AgNPs at the optimum condition have a good stability in suspension and within narrow size distribution. The present study demonstrates that RSM with CCD provide a reliable and accurate methodology for optimizing the gamma irradiation synthesis of alginate-stabilized AgNPs without addition of a hydroxyl scavenger.

ACKNOWLEDGMENT

This work was supported by Universitas Indonesia through PUTI Doctor Grant Contract No. NKB-567/UN2.RST/HKP.05.00/2020. Authors are also thankful for Research Center for Radiation Process Technology and Research Center for Nuclear Fuel Cycle and Radioactive Waste Technology, Research Organization for Nuclear Energy - National Research and Innovation Agency, Indonesia, for providing facility, space, and resource for this work.

AUTHOR CONTRIBUTION

Dian Pribadi Perkasa and Wawaimuli Arozal are the main contributors who conducted the experiment and developed the mathematical model. All authors contributed in data analysis and writing and revision of the manuscript. All authors approved the final version of this manuscript.

REFERENCES

1. H. Agarwal, A. Nakara and V. K. Shunmugam, *Biomed. Pharmacother.* **109** (2018) 2561.
2. M. D. Mauricio, S. Guerra-Ojeda, P. Machio *et al.*, *Oxid. Med. Cell. Longevity* **2018** (2018) 1.
3. K. Siczek, H. Zatorski, A. Chmielowiec-Korzeniowska *et al.*, *Pharmacol. Rep.* **69** (2017) 386.
4. X. Liu, P. Gao, J. Du *et al.*, *J. Pediatr. Surg.* **52** (2017) 2083.
5. K. Siczek, H. Zatorski, A. Chmielowiec-Korzeniowska *et al.*, *Chem. Biol. Drug Des.* **89** (2017) 538.
6. J. B. Krajewska, O. Długosz, M. Sałaga *et al.*, *Int. J. Pharm.* **585** (2020) 1.
7. N. Krishnan, B. Velramar, B. Ramatchandirin *et al.*, *Mater. Sci. Eng., C* **91** (2018) 146.
8. L. Xu, Y. Wang, J. Huang *et al.*, *Theranostics* **10** (2020) 8996.
9. L. N. Shirokova, A. A. Revina, V. A. Aleksandrova *et al.*, *Inorg. Mater. Appl. Res.* **7** (2016) 730.
10. S. M. Ghoreishian, S. Kang, G. S. R. Raju *et al.*, *Chem. Eng. J.* **360** (2019) 1390.
11. K. Čubová and V. Čuba, *Radiat. Phys. Chem. Oxf. Engl.* **158** (2019) 153.
12. E. B. Gracien, M. L. Jérémie, L. K. Joseph *et al.*, *SN Appl. Sci.* **1** (2019) 1.
13. Y. Liu, S. Chen, L. Zhong *et al.*, *Radiat. Phys. Chem.* **78** (2009) 251.
14. L. Agüero, D. Zaldivar-Silva, L. Peña *et al.*, *Carbohydr. Polym.* **168** (2017) 32.
15. A. Sosnik, *ISRN Pharm.* **2014** (2014) 1.
16. D. V. Phu, L. A. Quoc, N. N. Duy *et al.*, *Nanoscale Res. Lett.* **9** (2014) 162.
17. C. P. Meehan and R. S. Wightman, *J. Addict. Med.* **14** (2020) e264.
18. F. Dong, E. Valsami-Jones and J. Kreft, *J. Nanopart. Res.* **18** (2016) 259.
19. R. Amdoun, L. Khelifi, M. Khelifi-Slaoui *et al.*, *Iran. J. Biotechnol.* **16** (2018) e1339.
20. O. Karhan, O. B. Ceran, O. N. Sara *et al.*, *Ind. Eng. Chem. Res.* **56** (2017) 8180.

21. J. J. M. Moreno, A. P. Pol, A. S. Abad *et al.*, *Psicothema* **25** (2013) 500.
22. D. P. Perkasa, M. Y. Yunus, Y. Warastuti *et al.*, *Atom Indonesia* **47** (2021) 111. (in Indonesian)
23. A. Loiseau, V. Asila, G. Boitel-Aullen *et al.*, *Biosens.* **9** (2019) 1.
24. N. G. Bastús, J. Piella and V. Puntès, *Langmuir* **32** (2016) 290.
25. G. G. Flores-Rojas, F. López-Saucedo and E. Bucio, *Radiat. Phys. Chem.* **169** (2020) 107962.
26. R. Dwiastuti, D. C. A. Putri, M. Hariono *et al.*, *Indonesian J. Chem.* **21** (2021) 502.
27. E. P. Utomo, M. Marina, W. Warsito *et al.*, *Indonesian J. Chem.* **18** (2018) 235.
28. B. S. Anant and C. S. Pritamdas, *Curr. Bioact. Compd.* **15** (2019) 242.
29. V. Lakkim, M. C. Reddy, R. R. Pallavali *et al.*, *Antibiotics* **9** (2020).
30. D. P. Perkasa, Erizal, T. Purwanti *et al.*, *Indonesian J. Chem.* **18** (2018) 367.
31. S. Bhagyaraj and I. Krupa, *Mol.* **25** (2020) 1.
32. G. Z. S. Oliveira, C. A. P. Lopes, M. H. Sousa *et al.*, *Int. Nano Lett.* **9** (2019) 109.